



PII: S0008-6223(97)00011-0

SELF-MONITORING OF STRAIN AND DAMAGE BY A CARBON–CARBON COMPOSITE

S. WANG and D. D. L. CHUNG*

Composite Materials Research Laboratory, Furnas Hall, State University of New York at Buffalo, Buffalo,
NY 14260-4400, U.S.A.

(Received 26 November 1996; accepted in revised form 2 January 1997)

Abstract—A carbon–carbon composite was found to be able to sense its own damage and dynamic strain, as its electrical resistance increased irreversibly upon damage and increased reversibly upon tensile strain. Even damage after the first cycle of tensile loading within the elastic regime was detected. The reversible resistance increase upon cyclic tension was mainly due to dimensional changes, but it was partly due to a phenomenon that intensified as damage increased. The gage factor, which is the reversible part of the fractional resistance change per unit reversible strain, was 1.2–2.4. © 1997 Elsevier Science Ltd

Key Words—A. Carbon/carbon composite, carbon composites, D. electrical properties, fracture, elastic properties.

1. INTRODUCTION

Carbon–carbon composites with continuous carbon fibers are used for high-temperature aerospace structures, due to the high-temperature resistance of the carbon matrix in these composites. The carbon matrix, though much more high-temperature resistant than a polymer matrix, is much more brittle than a polymer matrix. This brittleness makes carbon–carbon composites prone to matrix cracking. As a result, there is a need for monitoring the condition or health of a carbon–carbon composite structure while the structure is in use, in order to minimise hazards. This monitoring is conventionally conducted by acoustic emission, which is capable of detecting substantial cracking, but not slight cracking. In contrast to this conventional approach, this paper addresses the use of the carbon–carbon composite itself as the damage sensor to monitor the composite's own damage (i.e. to self-monitor the damage), using the increase in electrical resistivity as a measure of the irreversible composite damage – even extremely slight damage.

A structure experiences reversible strain during use. The monitoring of the strain is useful for control of the structure, so as to make the structure “smart”. Embedded or attached strain sensors are conventionally used for the strain monitoring. These sensors can be optical fibers and a variety of strain gages. For a high-temperature structure, such as one made of a carbon–carbon composite, the sensors must be able to withstand high temperatures. Even if the temperature resistance is not a problem, the sensors suffer from poor durability and, in the case of embedded sensors, they have the tendency to degrade the mechanical properties of the structure. In contrast, in this paper we have employed the carbon–car-

bon composite itself as the strain sensor to monitor the composite's own strain (i.e. to self-monitor the strain), based on the reversible increase of the electrical resistivity of the composite upon tensile straining.

The combined ability to monitor both reversible strain and damage is particularly valuable in real-time fatigue damage monitoring under dynamic loading which may or may not be periodic in time, because the strain cycle and the point within the cycle at which damage occurs can be identified.

2. EXPERIMENTAL METHODS

The carbon–carbon composite, kindly provided by Sigril Great Lakes Carbon Corp. (Union, NJ) under the grade designation of CC 1501G, was in the form of a sheet containing carbon fiber roving fabric (90° biaxial weaving) and was produced by lamination and compression. The optical microscopic views of the top and edge of the laminate are shown in Fig. 1. The heat treatment temperature used in production was 2000°C. According to the manufacturer, the bulk density was 1.40–1.45 g cm⁻³, the open porosity was 20–25%, the bending strength was 210–250 MPa, the dynamic modulus of elasticity was 60–65 GPa, the interlaminar shear strength was 9–12 MPa and the ash content was 0.08%. According to our measurement, the tensile strength was ~382 MPa.

The electrical resistance R was measured in the direction of one of the two perpendicular sets of fibers using the four-probe method while cyclic and static tension until failure was applied in the same direction. Silver electrically conducting paint was used for all electrical contacts. The four probes consisted of two outer current probes and two inner voltage probes. The resistance R refers to the sample DC resistance between the inner probes. The four electrical contacts were placed around the whole

*Corresponding author.

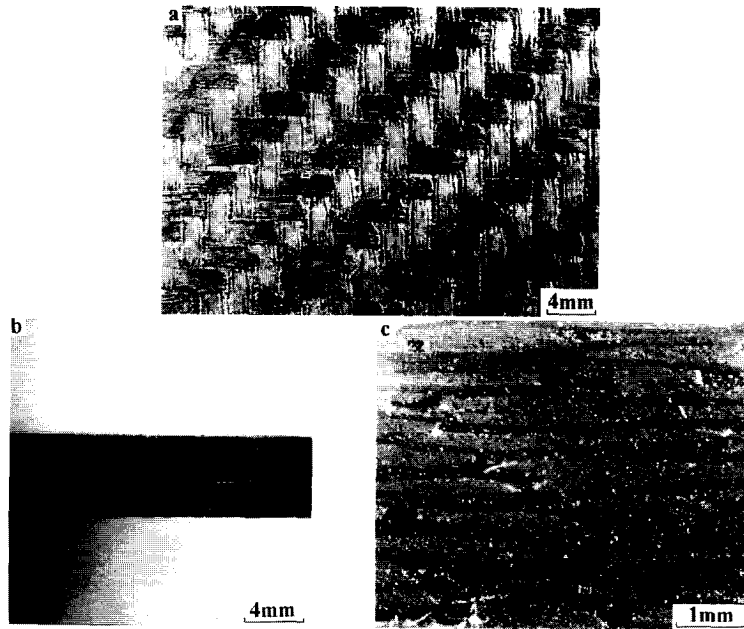


Fig. 1. Optical micrographs of the carbon-carbon composite. (a) Top view showing the weave pattern. (b,c) Edge view at two magnifications showing the fiber layers.

perimeter of the sample in four parallel planes that were perpendicular to the stress axis, such that the inner probes were 60 mm apart. The specimen was of length 85 mm, width 6.80 mm and thickness 2.46 mm. The stress axis was along the longest dimension of the specimen. One strain gage was attached to the center of one of the two opposite large surfaces of a specimen to measure the strain in the longitudinal direction. Two strain gages were attached to the centers of the two opposite large surfaces of a specimen to measure the strain in the lateral direction. Two other strain gages were attached to the two

opposite small surfaces to measure the strain in the thickness direction. The strains from each pair of strain gages were averaged. The average strains were used to calculate the Poisson's ratios in the lateral and thickness directions, ν_{12} and ν_{13} , respectively. A Keithley 2001 multimeter and a hydraulic mechanical testing system (MTS 810) were used.

3. RESULTS AND DISCUSSION

Figure 2 shows the stress (curve (a)) and the fractional resistance increase ($\Delta R/R_0$) (curve (b))

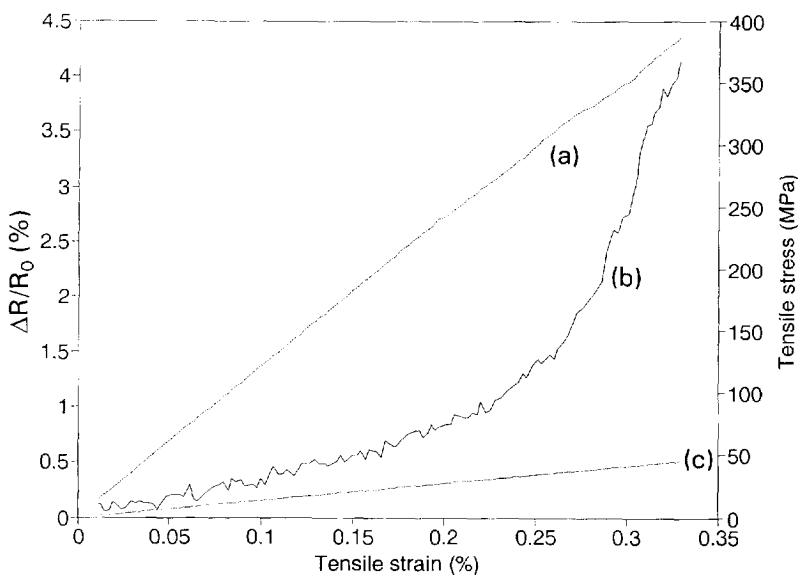


Fig. 2. Plots of (a) tensile stress vs strain, and (b) $\Delta R/R_0$ vs strain, obtained simultaneously during static tension up to failure. Curve (c) is the calculated $\Delta R/R_0$ based on dimensional changes.

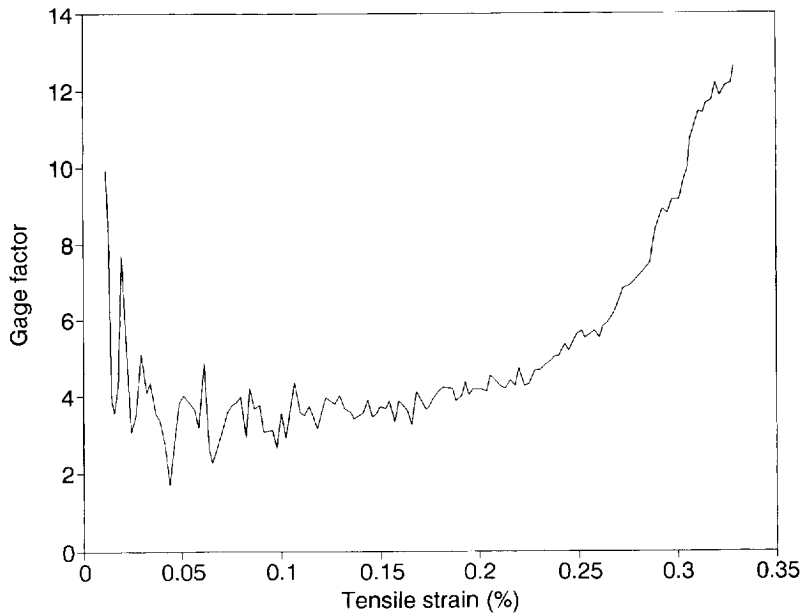


Fig. 3. Variation of the gage factor ($\Delta R/R_0$ per unit strain, from Fig. 2) with tensile strain.

obtained during static tension up to failure. $\Delta R/R_0$ increased monotonically with strain, such that the increase was gradual (only slightly above the increase in $\Delta R/R_0$ due to the changes in dimensions, curve (c) in Fig. 2) at low strains and abrupt at high strains. The corresponding gage factor as a function of strain is shown in Fig. 3. The gage factor was about 3.5 at low strains and increased at high strains.

Figure 4 shows $\Delta R/R_0$ obtained during cyclic tension to a stress amplitude (360 MPa) equal to 94% of the breaking stress. The tensile strain was almost totally reversible. The irreversible strain was 0.040% at the end of the first cycle, and increased very

slightly with increasing cycle number. $\Delta R/R_0$ increased upon loading in every cycle, such that it irreversibly increased slightly after every cycle and the irreversible increase in $\Delta R/R_0$ was particularly large for the first cycle, as shown in Fig. 4. As shown in Fig. 5, at fatigue failure, $\Delta R/R_0$ abruptly increased, such that $\Delta R/R_0$ did not more rapidly increase irreversibly near the end of fatigue life. Figure 6 shows the peak $\Delta R/R_0$ values in a cycle as a function of cycle number throughout the fatigue life up to failure. The peak $\Delta R/R_0$ increased with cycle number significantly during the first 500 cycles and gradually during all subsequent cycles up to failure. The small step

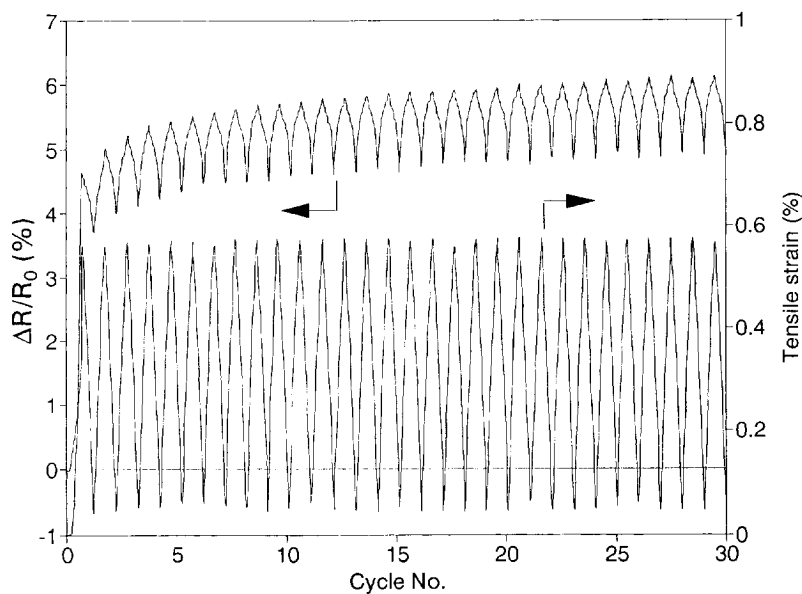


Fig. 4. Plots of $\Delta R/R_0$ vs cycle no. and of tensile strain vs cycle no., obtained simultaneously during first cycle tension at a stress amplitude of 94% of the fracture stress.

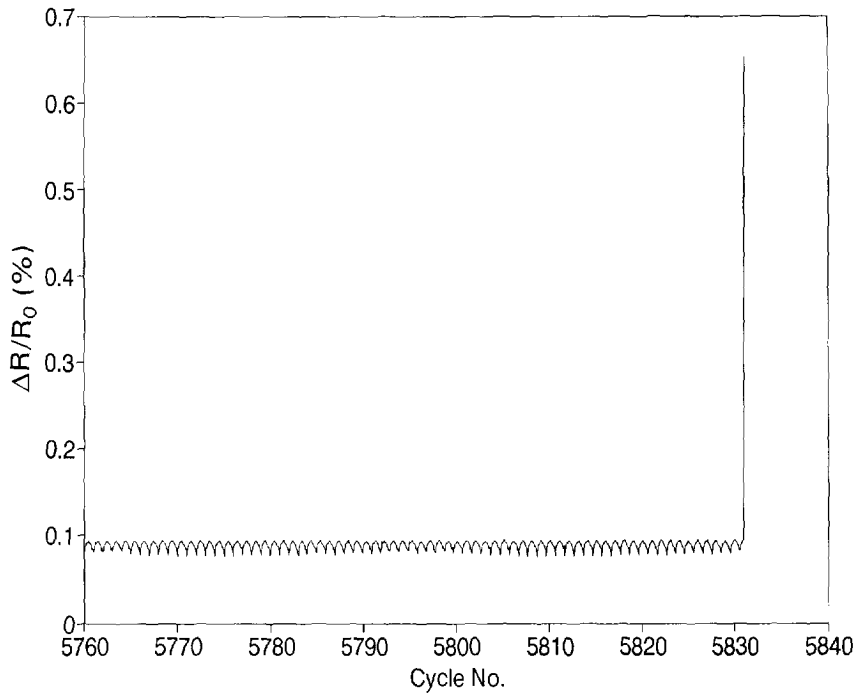


Fig. 5. Plot of $\Delta R/R_0$ vs cycle no. during cyclic tension from cycle 5760 to end of fatigue life (at 5831 cycles) at a stress amplitude of 94% of the fracture stress.

increases in the peak $\Delta R/R_0$, for example at ~ 1350 cycles, are not experimental artifacts but are attributed to damage occurring at those cycle numbers, similar to the step increases observed for a continuous carbon fiber polymer-matrix composite under similar cyclic loading [1].

Measurement of $\Delta R/R_0$ during cyclic tension was performed up to cycle 2000 (except for the highest stress amplitude of 97% of the fracture stress, at

which fatigue failure occurred at cycle 22) at various stress amplitudes and the results are shown in Table 1. The reversible part of $\Delta R/R_0$ increased significantly with increasing stress amplitude, and less significantly with increasing cycle number, as shown in both Table 1 and Fig. 7. The irreversible part of $\Delta R/R_0$ at the lowest stress amplitude (30% of fracture stress), but exceeded the reversible part of $\Delta R/R_0$ at higher

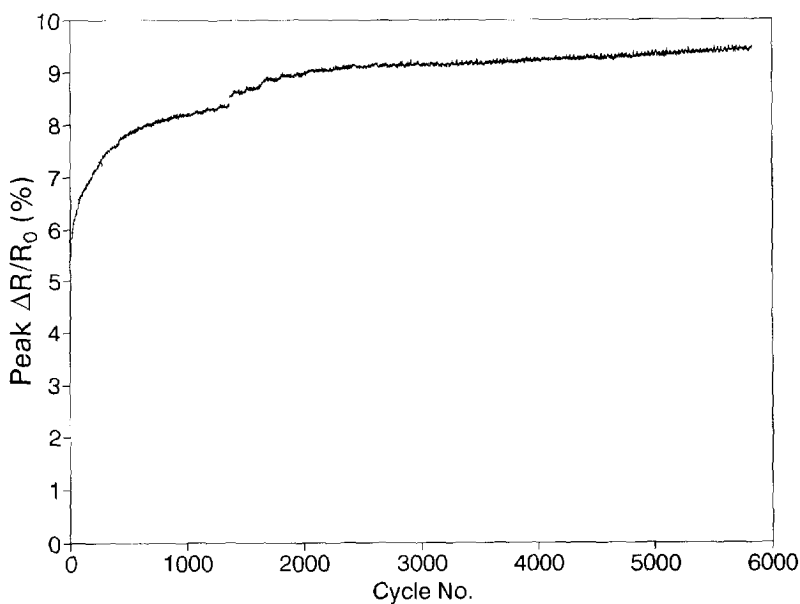


Fig. 6. Variation of the peak $\Delta R/R_0$ with cycle no. throughout the entire fatigue life at a stress amplitude of 94% of the fracture stress.

Table 1. $\Delta R/R_0$, strain gage factor and modulus obtained during cyclic tension at various stress amplitudes

Maximum stress (MPa) (± 1)		114	190	266	342	355	370	
Maximum stress/fracture stress		0.30	0.50	0.70	0.90	0.93	0.97	
$\Delta R/R_0$ (%) (± 0.001)								
Reversible	Cycle	1	0.185	0.230	0.331	0.442	0.639	0.968
	Cycle	2	0.173	0.222	–	0.477	0.762	1.090
	Cycle	20	0.171	0.221	0.335	0.510	0.913	1.203
	Cycle	100	0.185	0.238	0.360	0.541	1.021	–
	Cycle	200	0.186	0.251	0.343	0.602	1.030	–
	Cycle	300	0.185	0.243	0.331	0.622	1.139	–
	Cycle	2000	0.197	0.243	0.342	0.620	1.204	–
Irreversible	Cycle	1	0.048	0.220	0.403	0.642	2.632	4.228
	Cycle	2	0.060	0.228	–	0.729	2.841	4.228
	Cycle	20	0.062	0.276	0.552	0.938	3.390	5.452
	Cycle	100	0.073	0.321	0.631	1.220	3.978	–
	Cycle	200	0.072	0.379	0.690	1.283	4.211	–
	Cycle	300	0.072	0.402	0.719	1.342	4.253	–
	Cycle	2000	0.073	0.448	0.748	1.384	4.463	–
Strain (%) (± 0.001)								
Reversible	Cycle	1	–	0.180	0.256	0.322	0.459	–
	Cycle	2	–	0.180	0.256	0.329	0.468	–
	Cycle	20	–	0.180	0.256	0.331	0.486	–
	Cycle	100	–	0.183	0.256	0.336	0.487	–
	Cycle	200	0.111	0.184	0.255	0.338	0.490	–
	Cycle	300	0.111	0.183	0.256	0.341	0.491	–
	Cycle	2000	0.111	0.184	0.255	0.344	0.494	–
Irreversible	Cycle	1	–	0.002	0.009	0.000	0.024	–
	Cycle	2	–	0.002	0.009	0.000	0.024	–
	Cycle	20	–	0.002	0.009	0.004	0.030	–
	Cycle	100	–	0.002	0.010	0.007	0.057	–
	Cycle	200	0.003	0.002	0.010	0.008	0.079	–
	Cycle	300	0.003	0.002	0.010	0.010	0.090	–
	Cycle	2000	0.003	0.003	0.015	0.010	0.106	–
Gage factor (± 0.01)								
	Cycle	1	–	1.28	1.29	1.37	1.39	–
	Cycle	2	–	1.23	–	1.45	1.63	–
	Cycle	20	–	1.23	1.31	1.54	1.88	–
	Cycle	100	–	1.30	1.41	1.61	2.10	–
	Cycle	200	1.68	1.36	1.35	1.78	2.10	–
	Cycle	300	1.67	1.33	1.29	1.82	2.32	–
	Cycle	2000	1.77	1.32	1.34	1.80	2.44	–
$\Delta R/R_0$ (%) due to reversible dimensional change (± 0.01) ^a								
	Cycle	1	–	0.28	0.39	0.50	0.71	–
	Cycle	2	–	0.28	0.39	0.51	0.72	–
	Cycle	20	–	0.28	0.39	0.51	0.75	–
	Cycle	100	–	0.28	0.39	0.52	0.75	–
	Cycle	200	0.17	0.28	0.39	0.52	0.76	–
	Cycle	300	0.17	0.28	0.39	0.53	0.76	–
	Cycle	2000	0.17	0.28	0.39	0.53	0.76	–
Secant modulus (GPa) (± 1)								
	Cycle	1	–	106	104	106	101 ^b 79	–
	Cycle	2	–	106	104	104	77	–
	Cycle	20	–	106	104	103	74	–
	Cycle	100	–	104	104	102	74	–
	Cycle	200	103	103	104	101	74	–
	Cycle	300	103	104	104	100	73	–
	Cycle	2000	103	103	104	99	73	–

^a $\Delta R/R_0$ (%) due to reversible dimensional change was calculated by: $\Delta R/R_0 = [(1 + \nu_{12} + \nu_{13})\epsilon] / [1 - (\nu_{12} + \nu_{13})\epsilon]$, where ϵ is the reversible strain, ν_{12} and ν_{13} are the Poisson's ratios. ($\nu_{12} = 0.11$, $\nu_{13} = 0.43$, as separately measured.)

^bTangent modulus during the first loading before the abrupt modulus drop.

stress amplitudes. The irreversible part of $\Delta R/R_0$ increased with stress amplitude much more significantly than the reversible part of $\Delta R/R_0$ for the whole range of stress amplitudes studied. As the stress amplitude was increased beyond 90% of the fracture stress, both the reversible part (Fig. 7) and irreversible part (Fig. 8) of $\Delta R/R_0$ increased abruptly. Both

the reversible and irreversible parts of $\Delta R/R_0$ increased with cycle number, but the effect was small compared to the effect of the stress amplitude (Table 1, Figs 7 and 8). The reversible strain increased with increasing stress amplitude linearly up to a stress amplitude of 90% of the fracture stress and abruptly increased upon further increase of the

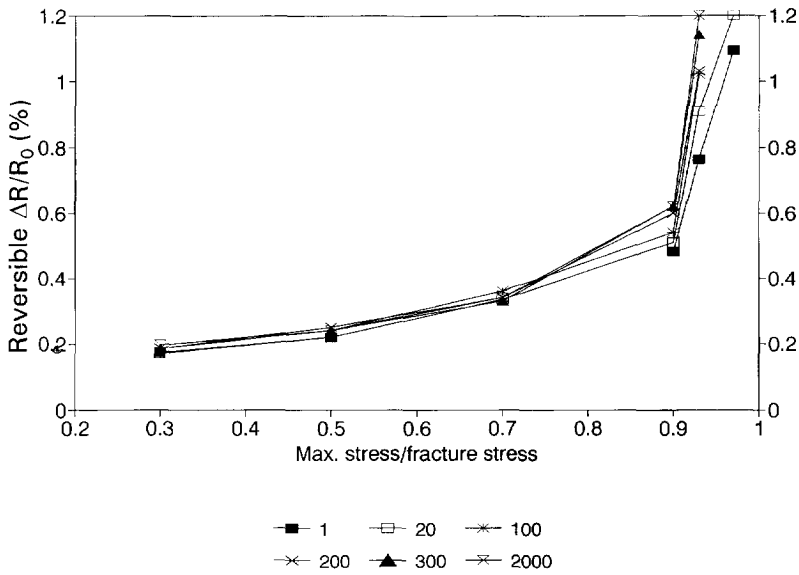


Fig. 7. Variation of the reversible part of $\Delta R/R_0$ with stress amplitude (fraction of fracture stress) for various fixed cycle numbers (i.e. 1, 20, 100, 200, 300 and 2000).

stress amplitude (Fig. 9). The magnitude of the irreversible strain was much lower than that of the reversible strain at all stress amplitudes (Table 1). Both reversible and irreversible strains increased with cycle number, but the effect of both is small compared to the effect of the stress amplitude (Table 1).

Figure 10 shows the relationships between $\Delta R/R_0$ (reversible and irreversible) and reversible strain at a fixed cycle number (2000). The reversible part of $\Delta R/R_0$ (curve (b)) exceeded the calculated $\Delta R/R_0$ (based on the reversible dimensional changes, curve (c)) when the reversible strain exceeded 0.35%. The irreversible part of $\Delta R/R_0$ (curve (a)) exceeded the reversible part of $\Delta R/R_0$ at all strains other than the

lowest (0.11%). In particular, it greatly exceeded the reversible part of $\Delta R/R_0$ when the reversible strain exceeded 0.35%. The gage factor, as given by the reversible part of $\Delta R/R_0$ per unit reversible strain, increased monotonically with increasing reversible strain for cycle numbers up to 100 (Table 1 and Fig. 11). At cycle 200 and beyond (at least up to cycle 2000), it decreased with increasing reversible strain at reversible strains less than 0.2% and increased with further increase in reversible strain (Table 1 and Fig. 12). The decrease in the gage factor at low reversible strains is probably an artifact due to the error in the very small values of reversible strain. The gage factor values were all below those

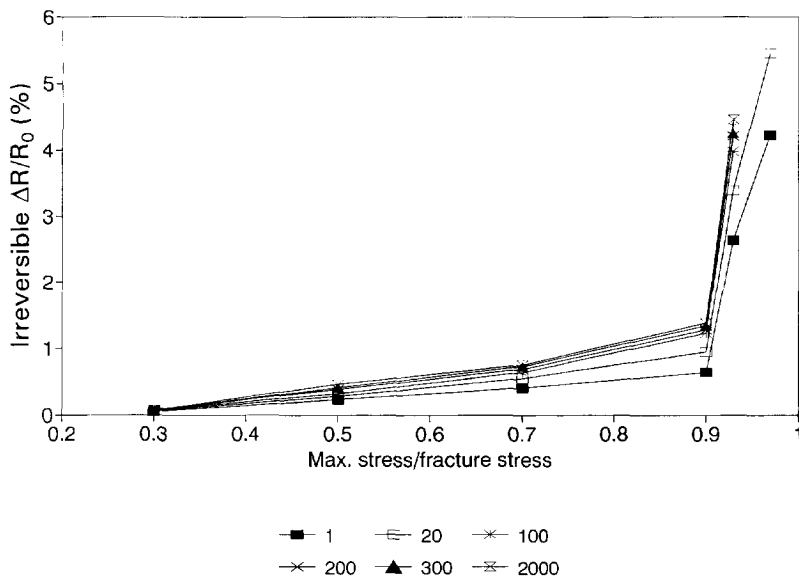


Fig. 8. Variation of the irreversible part of $\Delta R/R_0$ with stress amplitude (fraction of fracture stress) for various fixed cycle numbers (i.e. 1, 20, 100, 200, 300 and 2000).

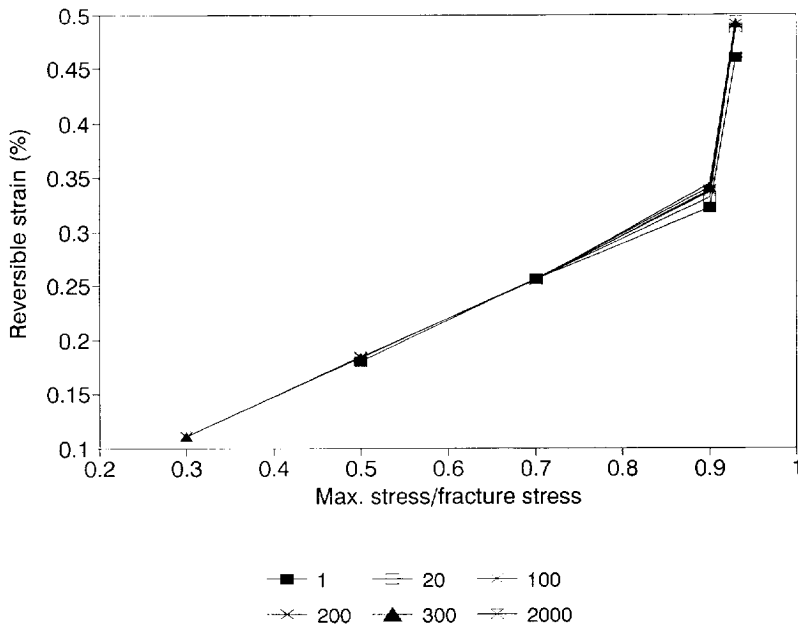


Fig. 9. Variation of the reversible strain with stress amplitude (fraction of fracture stress) for various fixed cycle numbers (i.e. 1, 20, 100, 200, 300 and 2000).

obtained from static tension (Fig. 3), in which the gage factor was obtained by dividing the total $\Delta R/R_0$ by the total strain. The secant modulus obtained at the maximum stress decreased with increasing stress amplitude and with increasing cycle number (Table 1), but the effect was very small, particularly when the stress amplitude was $\leq 70\%$ of the fracture stress. However, as shown in the stress-strain curves obtained during cyclic loading at a stress of 93% of the fracture stress (Fig. 13), the tangent modulus during the first loading (101 GPa) was higher than the secant modulus during first

unloading (79 GPa) and subsequent loading and unloading (Table 1). The stress-strain curves during first unloading and subsequent loading and unloading essentially overlapped and were not linear. The non-linearity was such that the slope increased with increasing strain; this is attributed to the stretching of the longitudinal woven fibers in the composite. This stretching is expected to occur more easily when the matrix is damaged. The abrupt decrease in tangent modulus during the first loading (Fig. 13) is attributed to damage; it was not observed at lower stress amplitudes, but is consistent with the big jump

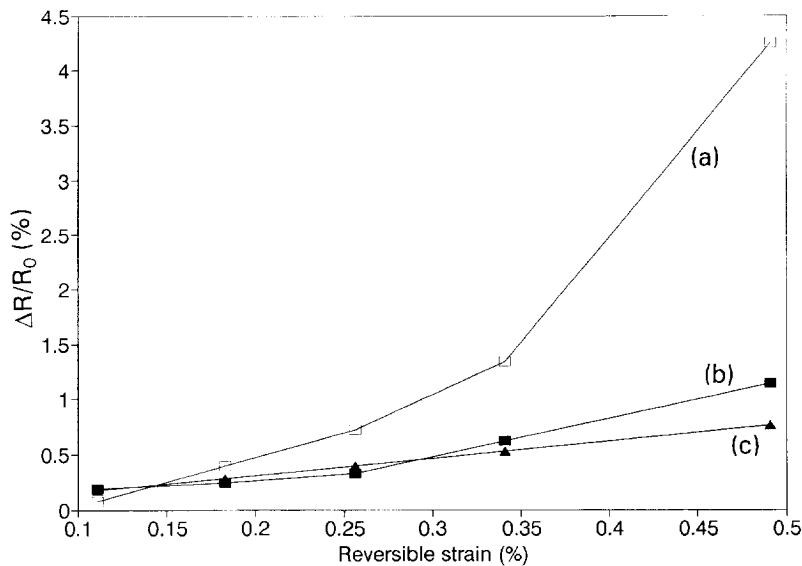


Fig. 10. Variation of $\Delta R/R_0$ with reversible strain for cycle 2000. (a) Irreversible part of $\Delta R/R_0$. (b) Reversible part of $\Delta R/R_0$. (c) Calculated $\Delta R/R_0$ based on reversible dimensional changes.

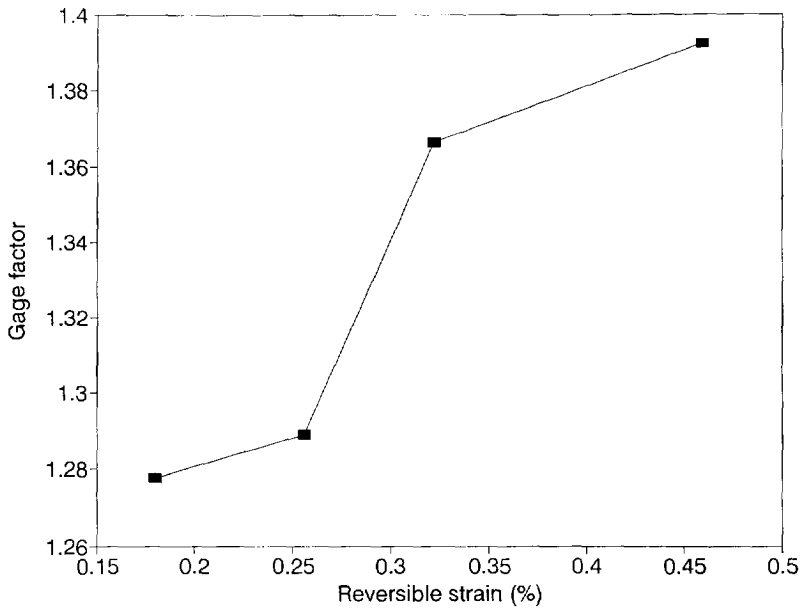


Fig. 11. Variation of gage factor (reversible part of $\Delta R/R_0$ per unit reversible strain) with reversible strain for cycle 1.

in the irreversible part of $\Delta R/R_0$ when the stress amplitude changed from 90 to 93% of the fracture stress (Table 1).

The reversible part of $\Delta R/R_0$ is mainly due to reversible dimensional changes and correlates with reversible strain. The irreversible part of $\Delta R/R_0$ is due to damage. Although the decreases in irreversible strain and modulus also indicate damage, the changes in these parameters are very small compared to the change in the irreversible part of $\Delta R/R_0$. The great sensitivity of the irreversible part of $\Delta R/R_0$ to damage is also shown by the significant non-zero value of the irreversible part of $\Delta R/R_0$ after merely the first cycle,

even at a stress amplitude of just 20% of the fracture stress (Fig. 14). However, the incremental rise in irreversible $\Delta R/R_0$ beyond ~ 500 cycles was small. The composite damage probably involved fiber-matrix interface weakening, matrix cracking and fiber breakage; these origins of damage could not be distinguished through the experimental technique used. Nevertheless, the increase of the irreversible part of $\Delta R/R_0$ as cycling progressed provided a continuous indication of the extent of damage. That the reversible part of $\Delta R/R_0$ also increased with cycling and that an abrupt increase of the irreversible part of $\Delta R/R_0$ is associated with an abrupt increase

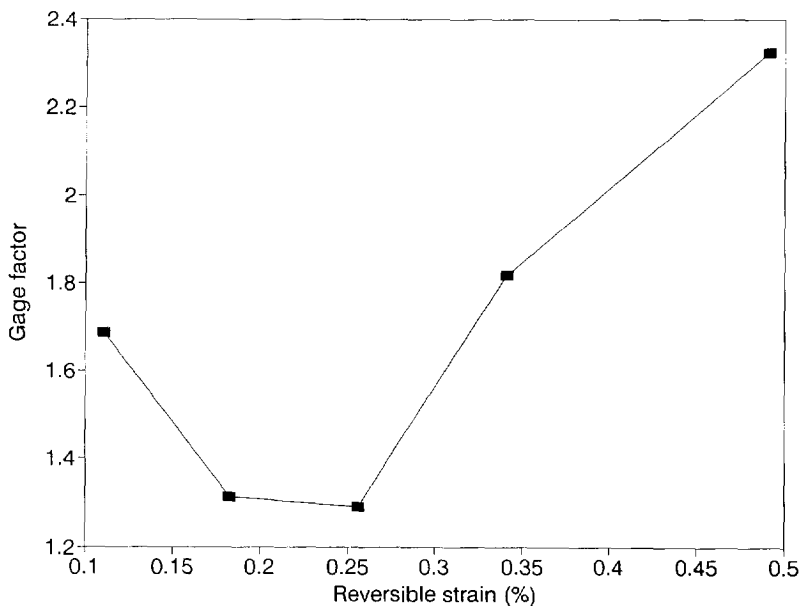


Fig. 12. Variation of gage factor (reversible part of $\Delta R/R_0$ per unit reversible strain) with reversible strain for cycle 2000.

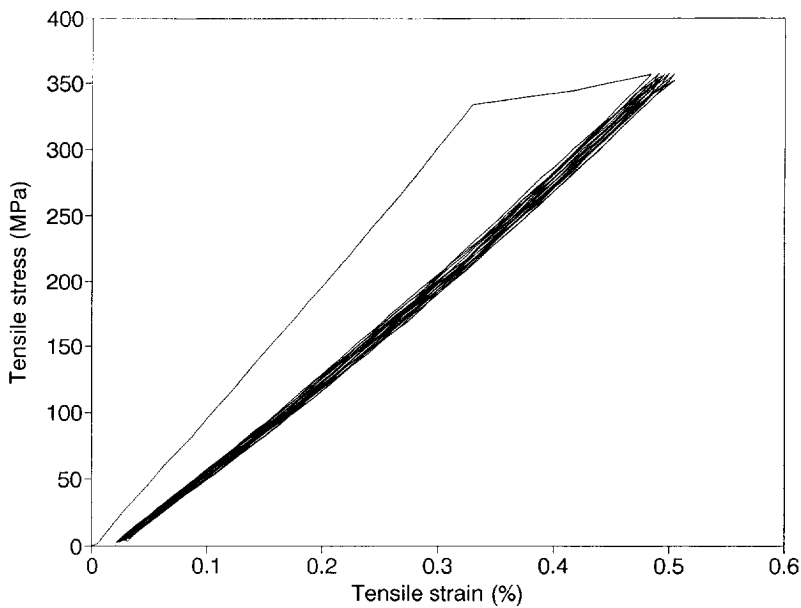


Fig. 13. Tensile stress-strain curves obtained during the first ten cycles at a stress amplitude equal to 93% of the fracture stress.

in the reversible part of $\Delta R/R_0$ (Figs 7 and 8) suggest that the reversible part of $\Delta R/R_0$ is partly associated with a phenomenon which intensifies as damage increases, although it is mostly associated with dimensional changes. This phenomenon may be reversible crack opening during tension, as cracks are expected to increase in size and/or density as cycling progresses. This interpretation is consistent with the observation that an abrupt increase in the reversible part of $\Delta R/R_0$ is associated with an abrupt increase in reversible strain (Figs 7 and 9) and that the abrupt increase in reversible strain occurs at stress amplitudes beyond the range in which the reversible strain is linear in relation to the stress amplitude (Fig. 8). As a result of this phenomenon, the gage factor

(reversible $\Delta R/R_0$ per unit reversible strain) increases slightly with cycle number. The dependence of the gage factor on the cycle number complicates the practical use of the carbon-carbon composite as a strain sensor.

The damage sensitivity of self-monitoring carbon-carbon composites is superior to that of self-monitoring continuous carbon fiber epoxy-matrix composites [1,2], which, through resistance measurement in the fiber direction, provide damage self-monitoring ability through the irreversible resistivity increase associated with fiber breakage alone [2,3]. Due to the insulating character of the epoxy matrix, the epoxy-matrix composite's resistivity in the fiber direction is essentially not affected by matrix damage.

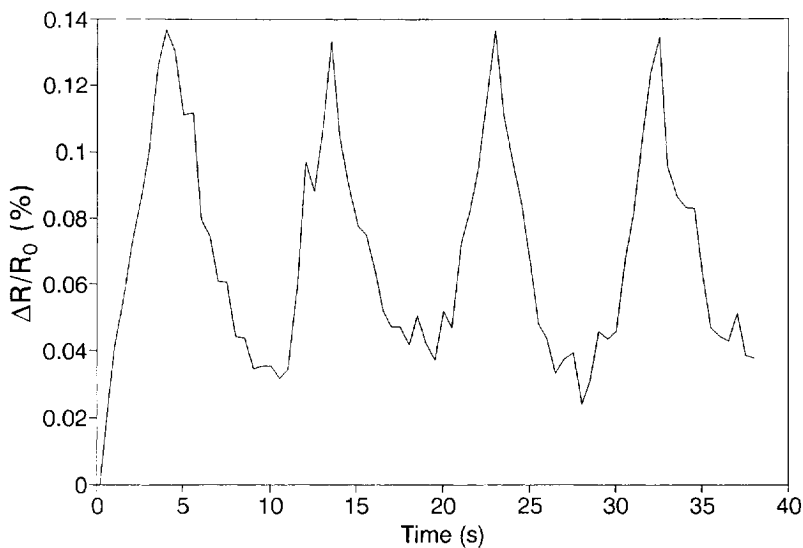


Fig. 14. Plot of $\Delta R/R_0$ vs time during the first four cycles at a stress amplitude of 20% of the fracture stress.

In contrast, the carbon matrix is electrically conducting, so it also allows matrix damage to be monitored electrically. Fatigue damage starts to be detectable electrically in the epoxy-matrix composite at about 50% of the fatigue life [1], but it is detectable in the carbon-carbon composite from the very first loading cycle onward, i.e. for the entire fatigue life. Fatigue self-monitoring had been reported in a CaF_2 -matrix SiC-whisker composite [4], but without dynamic strain monitoring. Self-monitoring by electrical resistance measurement, at least in the case of carbon-carbon composites, is better than acoustic emission [5,6] in damage sensitivity, as acoustic emission does not detect the damage until it is significant.

The strain sensitivity of self-monitoring carbon-carbon composites is much inferior to that of self-monitoring continuous carbon fiber epoxy-matrix composites, which provide strain self-monitoring ability through the reversible resistivity decrease parallel to the fibers due to increase in the degree of fiber alignment upon tensile loading parallel to the fibers [2]. The strain sensitivity (i.e. the gage factor), expressed as the fractional increase in resistance ($\Delta R/R_0$) per unit reversible strain, is -36 for the epoxy-matrix composite [2] and 1.2–2.4 for the carbon-carbon composite.

The gage factor of the carbon-carbon composite is about equal to that of a single bare carbon fiber [7–12], which also increases in resistance upon tension due mainly to dimensional changes. However, a single carbon fiber [3] is not as effective a damage sensor as a carbon-carbon composite, since matrix cracking and fiber-matrix interface weakening cannot occur in a single carbon fiber.

4. CONCLUSION

A carbon-carbon composite was found to be able to sense its damage and dynamic strain through

changes in its DC electrical resistance. The resistance increased irreversibly due to damage and increased reversibly upon tensile straining in the elastic regime. The damage sensitivity was so high that even the damage after the first cycle of tensile loading within the elastic regime was detected. The continuous increase in the irreversible $\Delta R/R_0$ as cycling progressed provided continuous monitoring of the extent of fatigue damage, although various extents of damage before cycle ~ 500 could be distinguished more clearly than those after cycle ~ 500 . The reversible resistance increase upon reversible straining was mainly due to dimensional changes, but it was partly due to a phenomenon (probably reversible crack opening) that intensified as damage increased. The strain gage factor was 1.2–2.4.

REFERENCES

1. Wang, X. and Chung, D. D. L., *Smart Mater. Struct.*, to be published.
2. Wang, X. and Chung, D. D. L., *Smart Mater. Struct.*, to be published.
3. Muto, N., Yanagida, H., Miyayama, M., Nakatsuji, T., Sugita, M., Ohtsuka, Y., *J. Ceramic. Soc. Japan*, **100**, (4), 585.1992.
4. Ishida, A., Miyayama, M., Yanagida, H., *J. Am. Ceram. Soc.*, **77**, (4), 1057.1994.
5. Konzstowicz, K. J., Fontaine, D., *J. Am. Ceramic Soc.*, **73**, (10), 2809.1990.
6. Santos-Leal, E., Lopez, R. J., *Measurement Science and Technology*, **6**, (2), 188.1995.
7. Conor, P. C., Owston, C. N., *Nature*, **223**, 1146.1969.
8. Wang, X. and Chung, D. D. L., *Carbon*, to be published.
9. Crasto, A. S. and Kim, R. Y., *Proc. Am. Soc. Composites*, 8th Tech. Conf., Technomic Pub. Co., Lancaster, PA, 1994, pp. 162–173.
10. Owston, C. N., *J. Phys. D*, **3**, 1615.1970.
11. Berg, C. A., Cumpston, H., Rinsky, A., *Textile Research Journal*, **42**, (8), 486.1972.
12. DeTeresa, S. J., *Carbon*, **29**, (3), 397.1991.